Multi-scale modeling of heterogeneous materials

M. Šejnoha[1] **and J. Šejnoha**

Czech Technical University in Prague
Faculty of Civil Engineering
Thákurova 7, 166 29, Prague

Key words: multi-scale modeling, woven composites, reinforced soils.

Abstract

The present paper addresses novel approaches in the analyses of complex material systems currently at the forefront of interest among civil engineers. Both traditional composites as well as recently emerged reinforced soils have been receiving much attention in the last decade. Although substantially different in their macroscopic response to various loading conditions, these materials are linked through complex geometries when viewed under a microscope, revealing spatial inhomogeneity and phases of various scales, which make up the material microstructure. Multi-scale or hierarchical modeling offers means to bridge length-scale differences, ranging from the size scales of microns to large structures such as bridges or earth dams. Preliminary accomplishments by the authors and their coworkers in this field are reviewed accompanied by the research needs and possible directions to pursue in the future.

1 Introduction

The undoubtable benefits offered by composite materials such as high strength, light weight, non-corrosive properties, etc., have recently attracted many design engineers in the civil engineering industry, primarily in conjunction with rehabilitation and repair of concrete and masonry structures. A lucid discussion on this subject is given in the work of [Sejnoha, et al. (1999)]. The endless search for reliable and low cost structural and material systems resulted in inexpensive fabrication methods for ever larger parts, which have made composites affordable for other applications such as the facade and structural parts of both commercial and industrial buildings and even bridges.

Among the most prominent material systems complying with the aforementioned requirements remain polymer matrix systems reinforced either by aligned fibers, whiskers or fabrics. The latter, in particular, is under continuous rise in civil infrastructure applications. They are typically supplied in the form of thick sandwich and laminated plates or laminated tubes supporting large compressive stresses. In this context the fiber waviness and misalignment play the main role in assessing the compressive strength of a laminate. This subject increases in proportion when realizing the complex microgeometry of such a composite. A sample of a graphite fiber fabric - polymer matrix composite system appears in Fig 1. This example clearly manifests the importance of multi-scale modeling starting from a

[1] Corresponding author – fax: ++420 2 24310775, e-mail: sejnom@fsv.cvut.cz

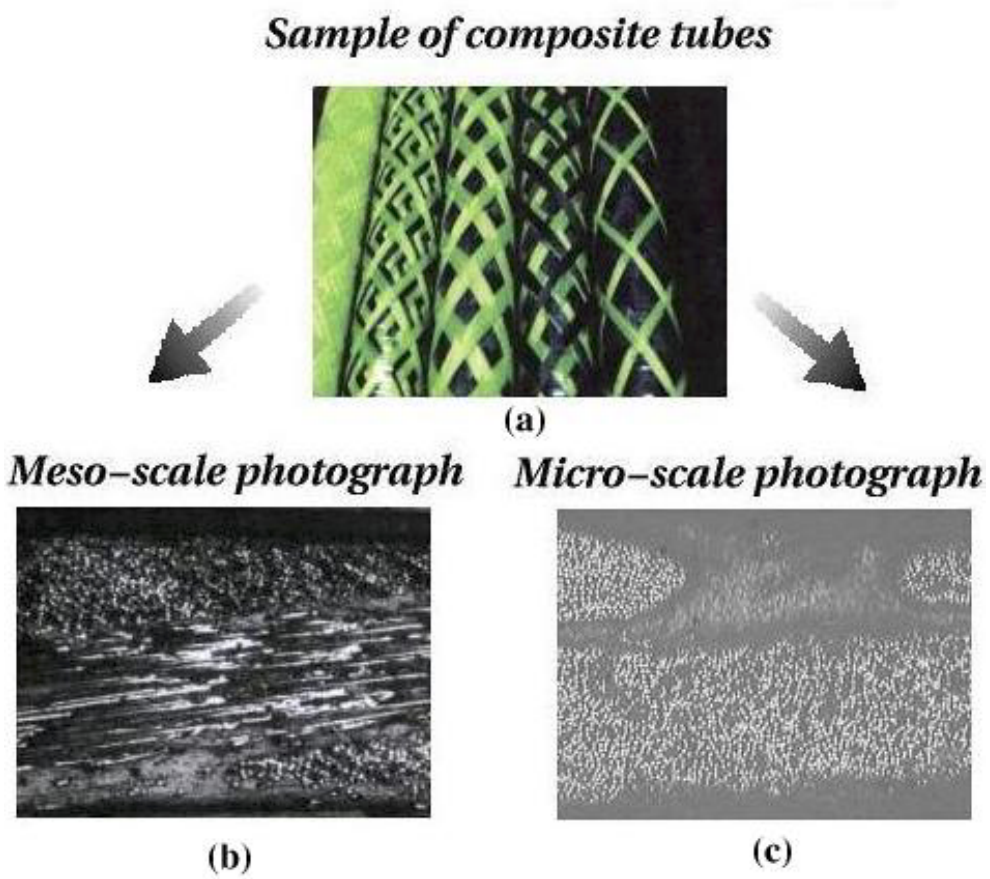

Figure 1: Graphite fiber fabric – polymer matrix composite

large structural element, e.g., a composite ply Fig. 1(a), having certain effective or macroscopic properties derived for the geometry specified on the meso-scale, Fig. 1(b). The classical problem of determining the effective elastic properties becomes even more complex when taking the level of the constituents, micro-scale Fig. 1(c), into consideration. Such a step creates demands for special techniques permitting the determination of the effective properties of disordered media. A vast body of literature has been devoted to this subject (see [Beran (1968), Drugan and Willis (1996), Torquato and Stell (1985)] to cite a few). Section 2 presents certain developments in this area.

The knowledge gained from years of experience with traditional composite materials has inspired geotechnical engineers to experiment with reinforced soils [Gray & Ohashi (1983), Tarliozs , et al. (1998)] with a focus on improving the shearing response of soils. In past practice a soil reinforcement has typically consisted of long flexible steel strips. In recent years, other types of reinforcements, such as synthetic or natural fibers, have gained increasing attention. From an environmental point of view, however, it becomes very important to address other types of potential materials produced by man and usually destined for landfill. The use of recycled polyethylene terephthalate (PET) material, which is mainly recovered from plastic soft drink bottles, is one of the possible sources.

This research area is at its dawn particularly in the context of randomly distributed fibers and much work has to be done. For example, a sufficient amount of information is lacking when

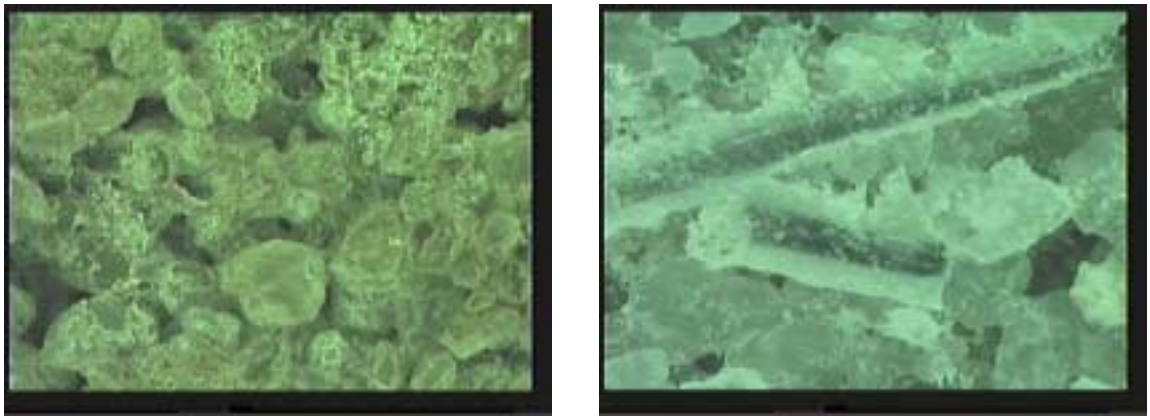

(a) (b)

Figure 2: A real micrograph of virgin (a) and reinforced (b) sand sample

taking into account the natural bond between the pore pressure and deformation of the skeleton-reinforcement mixture, which requires solving a coupled problem. As for traditional composites, useful information in developing a solid constitutive model can be gained from the knowledge of a real microstructure. Microscopic images of both virgin and reinforced quartz sand are displayed in Fig. 2. When transformed into binary images, they can serve to evaluate, e.g., skeleton volume fraction together with volume fraction and distribution of pores, and eventually to determine the fluid permeability of a soil using novel homogenization techniques [Torquato (1991)]. As for reinforced soils, the images taken from real material samples can be further used to assess the spatial distribution of reinforcements and to verify the degree of anchoring of reinforcements inside the soil body. Preliminary experimental results derived for soils reinforced by strips of polyethylene bottles are discussed in Section 3. These results further support the need for proper micro-macro analysis combined with image analysis.

2 Multi-scale modeling of woven composites

This section reviews certain directions currently pursued when dealing with composites. It has been recognized long ago that the overall response of composite materials in general and the woven composite structures in particular is highly influenced by the micromechanical behavior of the composite systems. As suggested in Fig. 1, such a research venture involves analyses on different scales.

2.1 Fiber tow

A multi-scale numerical model requires beginning at the first scale with a fiber and matrix mixture forming a fiber tow. Until recently, the simple averaging techniques were mostly used to generate the effective properties of this basic building element. However, since fibers are randomly distributed within the bundle and since this distribution is likely affected by the initial fiber pre-stress it is advisable to treat homogenization on this level from the

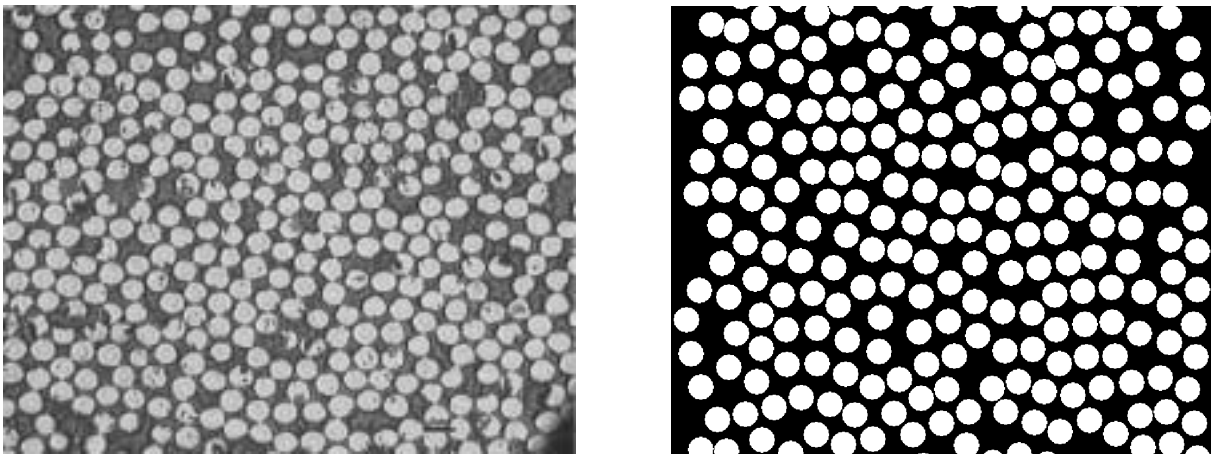

(a) (b)

Figure 3: A real micrograph of transverse plane section of a fiber tow and its binary image

point of view of probabilistic methods. Presently, a well-founded physical and mathematical basis for describing material statistics exists, including phase volume fractions and, at a minimum, the two-point probability function [Drugan and Willis (1996), Torquato and Stell (1985)]. This approach has been successfully implemented by [Zeman & Sejnoha (2001), Sejnoha, et al. (2000)] in an analysis of graphite fiber tow impregnated by polymer matrix. Much of the work characterizing the microstructure of heterogeneous materials now relies on the existence of images of real materials. The material system under consideration, as viewed under a scanning electron-microscope, appears in Fig. 3(a). Such a medium is evidently disordered and conventional periodic unit cell models such as the hexagonal array model [Teply and Dvorak (1988)] are not applicable. To provide for the lack of periodicity, one may incorporate various types of *n*-point statistical descriptors in an analysis of the disordered media. Such statistical descriptors introduce information beyond that contained in the volume fractions. It turns out that the two-point probability function S_{rs}, which gives the probability of finding two points $\mathbf{x}_1,\mathbf{x}_2$ randomly thrown into the media located in the phases r, s, is sufficient in determining the effective properties of the composite displayed in Fig. 3(a).

To evaluate this function we first generate a binary image of the real microstructure (see Fig. 3(b)). The sample is thus stored as a matrix of bits corresponding to values of either 0 (matrix phase) or 1 (fiber phase). Various algorithms can be used to assert the desired function from the digitized image of Fig. 3(a). To that end, we first form a sampling template (see Fig, 4(a)). The center of such a sampling template is randomly thrown into a digitized medium and corresponding successful hits are summed up and averaged. An example of the resulting function obtained when employing this procedure is shown in Fig. 4(b). This particular variation of S_{mm} corresponds to a random distribution of the graphite fibers shown in Fig. 3

Once this function is known we may generally proceed in two different ways. The first approach draws on the extended Hashin-Shtrikman (H-S) variational principle, while the second one relies on the existence of a suitable periodic unit cell.

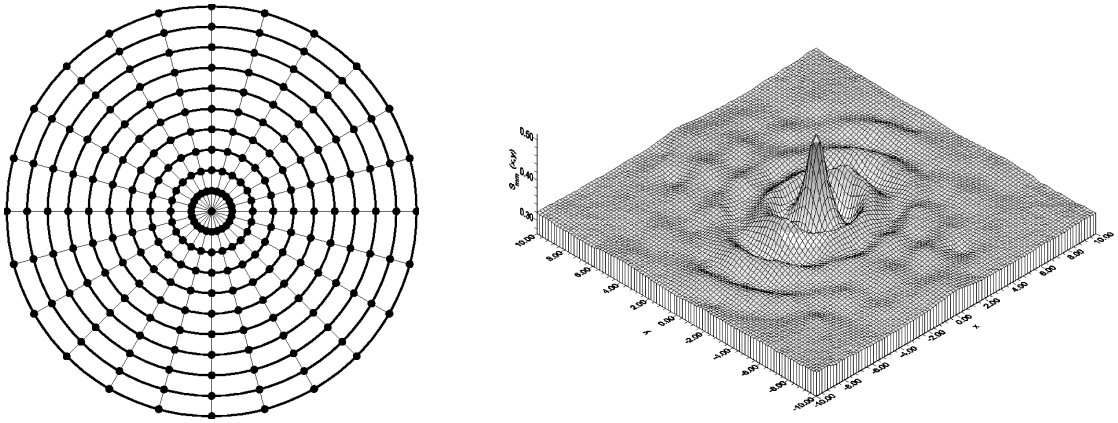

(a) (b)

Figure 4: Sampling template and two-point probability function $S_{mm}(\mathbf{x})$

2.1.1 Homogenization on a micro-scale using the H-S principle

Here, we focus on the theoretical aspects associated with the variational formulation for anisotropic and non-homogeneous bodies with prescribed displacements $\boldsymbol{u} = \overline{\boldsymbol{u}}$ along the entire boundary S of the composite. In addition, eigenstrains (stress-free strains) or eigenstresses are admitted in the present formulation. The generalized Hook law, including eigenstresses $\boldsymbol{\lambda}$, is then written as

$$\boldsymbol{\sigma}(\mathbf{x}) = \mathbf{L}(\mathbf{x})\boldsymbol{\varepsilon}(\mathbf{x}) + \boldsymbol{\lambda}(\mathbf{x}) \text{ in } \Omega\,, \ \boldsymbol{u} = \overline{\boldsymbol{u}} \text{ on } S\,. \tag{1}$$

Following the Hashin-Shtrikman idea [Hashin & Shtrikman (1963)], the local stresses in Eq. (1) are found from the solutions of two auxiliary problems, Fig. 5.

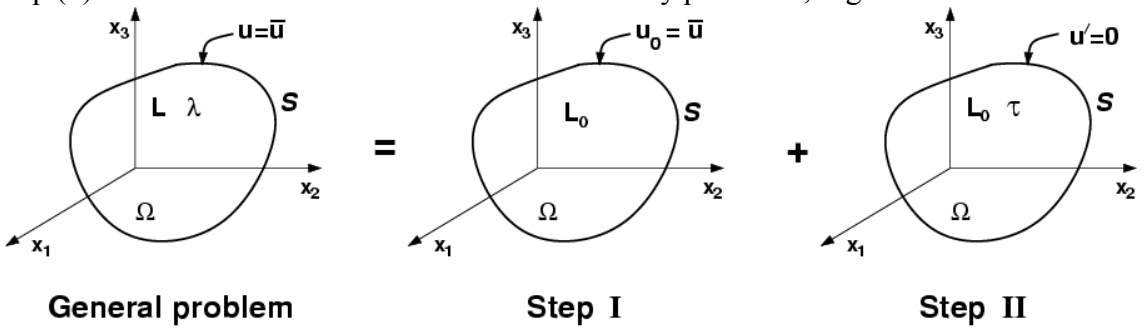

Figure 5: Body with prescribed surface displacements and eigenstresses

First, suppose that an affine displacement field $\boldsymbol{u}_0(\mathbf{x}) = \boldsymbol{E}\cdot\mathbf{x}$ is prescribed (Step I). The corresponding uniform strain $\boldsymbol{E}$ and stress $\boldsymbol{\Sigma}$ fields are related through constitutive law in the form

$$\boldsymbol{\Sigma} = \mathbf{L}_0\boldsymbol{E} \quad \text{in } \Omega, \quad \boldsymbol{u}_0 = \overline{\boldsymbol{u}} \quad \text{on } S, \tag{2}$$

where $\mathbf{L}_0$ is the material stiffness tensor of a homogeneous reference material.

Introducing the symmetric stress polarization tensor $\boldsymbol{\tau}$, the local stress $\boldsymbol{\sigma}(\mathbf{x})$ at point $\mathbf{x}$ in Ω of a composite is found by superimposing the solution of the local problem displayed in Fig. 5(Step II). Therefore

$$\boldsymbol{\sigma}(\mathbf{x}) = \mathbf{L}_0\boldsymbol{\varepsilon}(\mathbf{x}) + \boldsymbol{\tau}(\mathbf{x}). \tag{3}$$

In addition, denote

$$\boldsymbol{u}' = \boldsymbol{u} - \boldsymbol{u}_0 \ \text{ in } \Omega, \ \boldsymbol{u}' = \mathbf{0} \ \text{ on } S \tag{4}$$

and

$$\boldsymbol{\varepsilon}' = \boldsymbol{\varepsilon} - \boldsymbol{E} \ \text{ in } \Omega, \ \boldsymbol{\sigma}' = \boldsymbol{\sigma} - \boldsymbol{\Sigma} \ \text{ in } \Omega. \tag{5}$$

The objective is to formulate a variational principle describing the behavior of the nonhomogeneous and anisotropic material subjected to known eigenstresses and prescribed boundary displacements. A schematic representation of this problem is displayed in Fig. 5. Provided that both $\boldsymbol{\sigma}$ and $\boldsymbol{\Sigma}$ fields are statically admissible (see [Bittnar & Šejnoha (1996)]), the following equations have to be satisfied

$$\boldsymbol{\nabla}\cdot(\mathbf{L}_0\boldsymbol{\varepsilon} + \boldsymbol{\tau}) = \mathbf{0} \quad \text{in } \Omega, \tag{6}$$

$$\boldsymbol{\tau} - (\mathbf{L} - \mathbf{L}_0)\boldsymbol{\varepsilon} - \boldsymbol{\lambda} = \mathbf{0} \quad \text{in } \Omega, \tag{7}$$

$$\boldsymbol{u}' = \mathbf{0} \quad \text{on } S. \tag{8}$$

A formulation equivalent to Eqs. (6) and (7) may be obtained by performing a variation of the extended functional

$$U_\tau = \frac{1}{2}\int_\Omega \Big(\boldsymbol{E}^{\mathrm{T}}\boldsymbol{\Sigma} - (\boldsymbol{\tau}-\boldsymbol{\lambda})^{\mathrm{T}}(\mathbf{L}-\mathbf{L}_0)^{-1}(\boldsymbol{\tau}-\boldsymbol{\lambda}) - 2\boldsymbol{\tau}^{\mathrm{T}}\boldsymbol{E} - \boldsymbol{\varepsilon}'^{\mathrm{T}}\boldsymbol{\tau} - \boldsymbol{\lambda}^{\mathrm{T}}\mathbf{L}^{-1}\boldsymbol{\lambda}\Big)\mathrm{d}\mathbf{x}. \tag{9}$$

Setting

$$\delta U_\tau = -\frac{1}{2}\int_\Omega \Big\{2\delta\boldsymbol{\tau}^{\mathrm{T}}\Big[(\mathbf{L}-\mathbf{L}_0)^{-1}(\boldsymbol{\tau}-\boldsymbol{\lambda}) - \boldsymbol{\varepsilon}\Big] + \delta\boldsymbol{\tau}^{\mathrm{T}}\boldsymbol{\varepsilon}' - \delta\boldsymbol{\varepsilon}'^{\mathrm{T}}\boldsymbol{\tau}\Big\}\mathrm{d}\mathbf{x} = 0, \tag{10}$$

we find that Eq. (7) is one of the stationarity conditions of U_τ, while the second condition, Eq. (6), follows after recasting the remaining terms in the brackets. Finally, it can be proved

that the stationary value U_τ^S of the potential U_τ equals the actual potential energy stored in the anisotropic and heterogeneous body

$$U_\tau^S = \frac{1}{2}\int_\Omega (\boldsymbol{\varepsilon}-\boldsymbol{\mu})^{\mathrm{T}}\mathbf{L}(\boldsymbol{\varepsilon}-\boldsymbol{\mu})\,\mathrm{d}\mathbf{x}\,, \tag{11}$$

where $\boldsymbol{\mu} = -\mathbf{L}^{-1}\boldsymbol{\lambda}$ is the vector of eigenstrains (stress-free strains). The function U_τ attains its maximum $\left(\delta^2 U_\tau < 0\right)$ if $(\mathbf{L}-\mathbf{L}_0)$ is positive definite, and its minimum, if $(\mathbf{L}-\mathbf{L}_0)$ is negative definite.

To make use of the H-S functional, Eq. (9), or its variation, Eq. (10), one has to express $\boldsymbol{\varepsilon}'$ via the polarization tensor $\boldsymbol{\tau}$

$$\boldsymbol{\varepsilon}'(\mathbf{x}) = \boldsymbol{\varepsilon}(\mathbf{x}) - \boldsymbol{E} = \left[\boldsymbol{\varepsilon}_0^*\boldsymbol{\tau}\right], \tag{12}$$

where the operator $\left[\boldsymbol{\varepsilon}_0^*\boldsymbol{\tau}\right]$ is defined in [Šejnoha (2000)]. Subscript 0 is used to identify this operator with the homogeneous reference medium. Introducing an ensemble average of the local strain $\boldsymbol{\varepsilon}$

$$\overline{\boldsymbol{\varepsilon}(\mathbf{x})} = \boldsymbol{E} + \int_\Omega \boldsymbol{\varepsilon}_0^*(\mathbf{x}-\mathbf{x}')\overline{\boldsymbol{\tau}(\mathbf{x}')}\,\mathrm{d}\mathbf{x}'\,, \tag{13}$$

yields Eq. (9) in the form

$$\begin{aligned}\boldsymbol{U}_\tau \;=\; \frac{1}{2}\int_\Omega \Big[&\boldsymbol{E}^{\mathrm{T}}\boldsymbol{\Sigma} - (\boldsymbol{\tau}(\mathbf{x})-\boldsymbol{\lambda}(\mathbf{x}))^{\mathrm{T}}(\mathbf{L}(\mathbf{x})-\mathbf{L}_0)^{-1}(\boldsymbol{\tau}(\mathbf{x})-\boldsymbol{\lambda}(\mathbf{x})) - 2\boldsymbol{\tau}^{\mathrm{T}}(\mathbf{x})\overline{\boldsymbol{\varepsilon}(\mathbf{x})}\\ &-\boldsymbol{\tau}^{\mathrm{T}}(\mathbf{x})\int_\Omega \boldsymbol{\varepsilon}_0^*(\mathbf{x}-\mathbf{x}')\left(\boldsymbol{\tau}(\mathbf{x}') - 2\overline{\boldsymbol{\tau}(\mathbf{x}')}\right)\mathrm{d}\mathbf{x}' - \boldsymbol{\lambda}^{\mathrm{T}}(\mathbf{x})\mathbf{L}^{-1}(\mathbf{x})\boldsymbol{\lambda}(\mathbf{x})\Big]\,\mathrm{d}\mathbf{x}\,.\end{aligned} \tag{14}$$

The details are given in [Šejnoha (2000)]. If each of the phase r of randomly arranged composite is homogeneous with moduli $\mathbf{L}_r$, $r = 1,\ldots,n$, then the material stiffness matrix in the sample α can be expressed as [Drugan and Willis (1996)]

$$\mathbf{L}(\mathbf{x},\alpha) = \sum_{r=1}^{n}\mathbf{L}_r\chi_r(\mathbf{x},\alpha), \tag{15}$$

where χ_r is the characteristic function being equal to 1 if the r^{th} phase is identified at $\mathbf{x}$ and 0 otherwise. Following [Drugan and Willis (1996)] the ensemble average of $\mathbf{L}$ is

$$\overline{\mathbf{L}(\mathbf{x})} = \sum_{r=1}^{n}\mathbf{L}_r S_r(\mathbf{x}). \tag{16}$$

Similarly, the trial field for $\boldsymbol{\tau}$ and eigenstress $\boldsymbol{\lambda}$ at any point $\mathbf{x}$ located in the sample α are provided by

$$\boldsymbol{\tau}(\mathbf{x},\alpha)=\sum_{r=1}^{n}\boldsymbol{\tau}_r(\mathbf{x})\chi_r(\mathbf{x},\alpha),\quad \boldsymbol{\lambda}(\mathbf{x},\alpha)=\sum_{r=1}^{n}\boldsymbol{\lambda}_r(\mathbf{x})\chi_r(\mathbf{x},\alpha), \tag{17}$$

with the respective ensemble averages written as

$$\overline{\boldsymbol{\tau}(\mathbf{x})}=\sum_{r=1}^{n}\boldsymbol{\tau}_r(\mathbf{x})S_r(\mathbf{x}),\quad \overline{\boldsymbol{\lambda}(\mathbf{x})}=\sum_{r=1}^{n}\boldsymbol{\lambda}_r(\mathbf{x})S_r(\mathbf{x}). \tag{18}$$

To facilitate the solution of the present problem, the material is assumed to be ergodic and statistically homogeneous. Therefore,

$$\overline{\mathbf{L}}=\sum_{r=1}^{n}\mathbf{L}_r c_r,\ \overline{\boldsymbol{\tau}(\mathbf{x})}=\sum_{r=1}^{n}\boldsymbol{\tau}_r(\mathbf{x})c_r,\qquad \overline{\boldsymbol{\lambda}(\mathbf{x})}=\sum_{r=1}^{n}\boldsymbol{\lambda}_r(\mathbf{x})c_r. \tag{19}$$

Substituting Eqs. (19) into Eq. (14) yields the extended averaged form of the Hashin-Shtrikman principle

$$\begin{aligned}\overline{U_\tau} &= \frac{1}{2}\int_\Omega\left[\boldsymbol{E}^{\mathrm{T}}\boldsymbol{\Sigma}-\overline{\boldsymbol{\lambda}}^{\mathrm{T}}(\mathbf{x})\overline{\mathbf{L}}^{-1}(\mathbf{x})\overline{\boldsymbol{\lambda}}(\mathbf{x})\right]\mathrm{d}\mathbf{x} \\ &- \frac{1}{2}\sum_{r}\int_\Omega\left[c_r(\boldsymbol{\tau}_r(\mathbf{x})-\boldsymbol{\lambda}_r(\mathbf{x}))^{\mathrm{T}}(\mathbf{L}_r-\mathbf{L}_0)^{-1}(\boldsymbol{\tau}_r(\mathbf{x})-\boldsymbol{\lambda}_r(\mathbf{x}))-2c_r\boldsymbol{\tau}_r{}^{\mathrm{T}}(\mathbf{x})\overline{\boldsymbol{\varepsilon}(\mathbf{x})}\right]\mathrm{d}\mathbf{x} \\ &- \frac{1}{2}\sum_{r}\sum_{s}\int_\Omega\boldsymbol{\tau}_r(\mathbf{x})^{\mathrm{T}}\int_\Omega\boldsymbol{\varepsilon}_0^*(\mathbf{x}-\mathbf{x}')\left[S_{rs}(\mathbf{x}-\mathbf{x}')\boldsymbol{\tau}_s(\mathbf{x}')-2c_s\overline{\boldsymbol{\tau}(\mathbf{x}')}\right]\mathrm{d}\mathbf{x}'\,\mathrm{d}\mathbf{x}\end{aligned} \tag{20}$$

Performing a variation with respect to $\boldsymbol{\tau}_r(\mathbf{x})$ and using Eq. $(19)_2$ provides the extended form of the stationarity conditions

$$\begin{aligned}&(\mathbf{L}_r-\mathbf{L}_0)^{-1}\boldsymbol{\tau}_r(\mathbf{x})c_r-\sum_{s=1}^{n}\int_\Omega\boldsymbol{\varepsilon}_0^*(\mathbf{x}-\mathbf{x}')[S_{rs}(\mathbf{x}-\mathbf{x}')-c_rc_s]\boldsymbol{\tau}_s(\mathbf{x}')\,\mathrm{d}\mathbf{x}'= \\ &=\overline{\boldsymbol{\varepsilon}(\mathbf{x})}c_r+(\mathbf{L}_r-\mathbf{L}_0)^{-1}\boldsymbol{\lambda}_r(\mathbf{x})c_r,\qquad r=1,\ldots,n.\end{aligned} \tag{21}$$

Suppose that $\overline{\boldsymbol{\varepsilon}(\mathbf{x})}=\boldsymbol{E}$, $\boldsymbol{\lambda}_r(\mathbf{x})=\boldsymbol{\lambda}_r$, $\boldsymbol{\tau}_r(\mathbf{x})=\boldsymbol{\tau}_r$ for general n-phase composite medium. The system (21) then reduces to

$$(\mathbf{L}_r-\mathbf{L}_0)^{-1}\boldsymbol{\tau}_r c_r-\sum_{s=1}^{n}\mathbf{A}_{rs}\boldsymbol{\tau}_s=c_r\boldsymbol{E}+(\mathbf{L}_r-\mathbf{L}_0)^{-1}c_r\boldsymbol{\lambda}_r,\quad r=1,2,\ldots,n, \tag{22}$$

where microstructure-dependent matrices $\mathbf{A}_{rs}$ do not depend on $\mathbf{x}$ and are provided by

$$\mathbf{A}_{rs}\quad=\quad\int_\Omega\boldsymbol{\varepsilon}_0^*(\mathbf{x}-\mathbf{x}')[S_{rs}(\mathbf{x}-\mathbf{x}')-c_rc_s]\,\mathrm{d}\mathbf{x}'$$

$$= \int_\Omega \boldsymbol{\varepsilon}_0^*(\mathbf{x}-\mathbf{x}')S'_{rs}(\mathbf{x}-\mathbf{x}')\,\mathrm{d}\mathbf{x}' = \int_\Omega \boldsymbol{\varepsilon}_0^*(\mathbf{x})S'_{rs}(\mathbf{x})\,\mathrm{d}\mathbf{x}, \tag{23}$$

where S'_{rs} denotes the fluctuating part of S_{rs} under the no-long range orders hypothesis. The preceding formula can be further rewritten as

$$\begin{aligned}\mathbf{A}_{rs} &= \int_\Omega \boldsymbol{\varepsilon}_0^*(\mathbf{x})S'_{rs}(\mathbf{x})\,\mathrm{d}\mathbf{x} \\ &= \left[\int_\Omega \boldsymbol{\varepsilon}_0^*(\mathbf{x})S'_{rs}(\mathbf{x})e^{\mathrm{i}\mathbf{x}\cdot\boldsymbol{\xi}}\,\mathrm{d}\mathbf{x}\right]_{\boldsymbol{\xi}=\mathbf{0}} = F\left[\boldsymbol{\varepsilon}_0^*(\mathbf{x})S'_{rs}(\mathbf{x})\right]_{\boldsymbol{\xi}=\mathbf{0}},\end{aligned} \tag{24}$$

where the operator F represents the Fourier transform. The property of F provides

$$\mathbf{A}_{rs} = \frac{1}{(2\pi)^d}\left[\int_\Omega \tilde{\boldsymbol{\varepsilon}}_0^*(\boldsymbol{\xi}-\boldsymbol{\xi}')\tilde{S}'_{rs}(\boldsymbol{\xi}')\,\mathrm{d}\boldsymbol{\xi}'\right]_{\boldsymbol{\xi}=\mathbf{0}} = \frac{1}{(2\pi)^d}\int_\Omega \tilde{\boldsymbol{\varepsilon}}_0^*(-\boldsymbol{\xi}')\tilde{S}'_{rs}(\boldsymbol{\xi}')\,\mathrm{d}\boldsymbol{\xi}'. \tag{25}$$

Since $\tilde{\boldsymbol{\varepsilon}}_0^*(-\boldsymbol{\xi}) = \tilde{\boldsymbol{\varepsilon}}_0^*(\boldsymbol{\xi})$ we finally arrive at

$$\mathbf{A}_{rs} = \frac{1}{(2\pi)^d}\int_\Omega \tilde{\boldsymbol{\varepsilon}}_0^*(\boldsymbol{\xi}')\tilde{S}'_{rs}(\boldsymbol{\xi}')\,\mathrm{d}\boldsymbol{\xi}'. \tag{26}$$

Note that the Fourier transform $\tilde{\boldsymbol{\varepsilon}}_0^*$ can be obtained for any homogeneous anisotropic reference media (see [Šejnoha (2001)] Appendix C, Section C.4), which is not generally possible for function $\boldsymbol{\varepsilon}_0^*$ itself. Therefore, once we are able to compute the values of $\tilde{S}'_{rs}$ we may evaluate integral (26) by the appropriate numerical procedure such as the familiar Gaussian quadrature.

2.1.2 Homogenization based on periodic fields

The above approach has received considerable attention when the material deforms in proportion to the magnitude of the applied forces and temperature changes. Although this approach does not preclude a description of material behavior at strains beyond the elastic limit (the inelastic effect can be expressed in terms of eigenstrains), it is usually preferable to tackle such a problem with the help of a epresentative volume element defined in terms of a suitably chosen periodic unit cell (PUC). In [Zeman & Sejnoha (2001), Sejnoha, et al. (2000)], we attempted to generate the desired PUC, such that it possesses similar statistical properties as the original material, and therefore can be considered as its reasonable approximation. We argue that if the PUC has a statistically similar spatial distribution of fibers as the real microstructure, it will also possess similar thermomechanical properties. To that end, a suitable optimization problem was introduced, and the PUC was found by matching the two-point probability functions of the real microstructure and the unit cell. Two representatives of the periodic unit cell constructed for the graphite/epoxy material system are displayed in Fig. 5. A standard homogenization technique can be used to analyze such unit cells under various thermomechanical loading conditions.

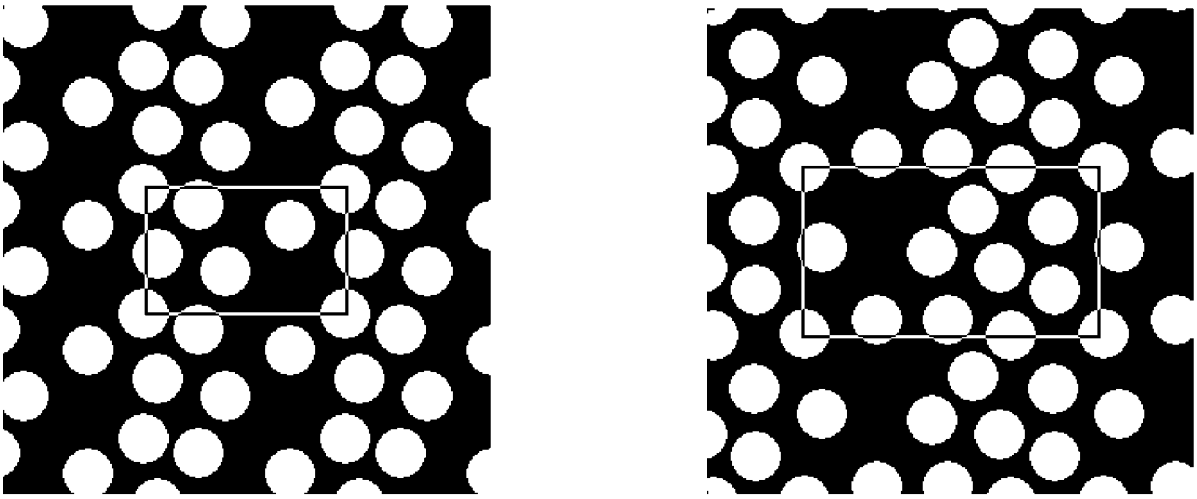

(a) (b)

Figure 6: Periodic unit cells: (a) 5-fiber PUC, (b) 10-fiber PUC

Here we limit our attention to pure mechanical loading and define the following mechanical loading problems

$$\boldsymbol{u}_0(\mathbf{x}) = \boldsymbol{E}\cdot\mathbf{x} \qquad \mathbf{x}\in S \tag{27}$$

$$\boldsymbol{p}_0(\mathbf{x}) = \boldsymbol{\Sigma}\cdot\boldsymbol{n}(\mathbf{x}) \qquad \mathbf{x}\in S \tag{28}$$

where $\boldsymbol{u}_0$ and $\boldsymbol{p}_0$ are the displacement and traction vectors on the external boundary S of a representative volume element Ω of the composite; $\boldsymbol{n}$ is the outer unit normal to S; $\boldsymbol{E}$ and $\boldsymbol{\Sigma}$ are the applied macroscopic uniform strain and stress fields, respectively. The macroscopic constitutive relations are then provided by

$$\langle\boldsymbol{\sigma}(\mathbf{x})\rangle = \langle\mathbf{L}(\mathbf{x})\boldsymbol{\varepsilon}(\mathbf{x})\rangle = \sum_{r=1}^{2} c_r\mathbf{L}_r\langle\boldsymbol{\varepsilon}_r(\mathbf{x})\rangle = \mathbf{L}\boldsymbol{E} \tag{29}$$

$$\langle\boldsymbol{\varepsilon}(\mathbf{x})\rangle = \langle\mathbf{M}(\mathbf{x})\boldsymbol{\sigma}(\mathbf{x})\rangle = \sum_{r=1}^{2} c_r\mathbf{M}_r\langle\boldsymbol{\sigma}_r(\mathbf{x})\rangle = \mathbf{M}\boldsymbol{\Sigma} \tag{30}$$

where $\langle\cdot\rangle$ stands for the spatial average of a given field, c_r is the volume fraction of the r^{th} phase, and $\mathbf{L}$ and $\mathbf{M}$ are the effective stiffness and compliance matrices of the heterogenous material, respectively. Eqs. (29) and (30) follow directly from Hill's lemma [Hill (1963)]. Hill proved that for compatible strain and equilibrated stress fields, the following relation holds

$$\left\langle\boldsymbol{\varepsilon}(\mathbf{x})^{\mathrm{T}}\boldsymbol{\sigma}(\mathbf{x})\right\rangle = \langle\boldsymbol{\varepsilon}(\mathbf{x})\rangle^{\mathrm{T}}\langle\boldsymbol{\sigma}(\mathbf{x})\rangle\,, \tag{31}$$

and consequently

$$\boldsymbol{E}^{\mathrm{T}}\mathbf{L}\boldsymbol{E} = \left\langle \boldsymbol{\varepsilon}(\mathbf{x})^{\mathrm{T}}\mathbf{L}(\mathbf{x})\boldsymbol{\varepsilon}(\mathbf{x})\right\rangle, \tag{32}$$

$$\boldsymbol{\Sigma}^{\mathrm{T}}\mathbf{M}\boldsymbol{\Sigma} = \left\langle \boldsymbol{\sigma}(\mathbf{x})^{\mathrm{T}}\mathbf{M}(\mathbf{x})\boldsymbol{\sigma}(\mathbf{x})\right\rangle. \tag{33}$$

Eq. (31) states in fact that the average of "microscopic" internal work is equal to the macroscopic work done by internal forces. The above relations provide the stepping stone for the derivation of the effective properties of composite materials.

The following paragraphs outline an evaluation of the effective properties of a composite aggregate represented here by the periodic material models of Fig. 6. Two specific approaches corresponding to loading conditions (27) and (28) are discussed in the sequel.

Formulation based on strain approach

Consider a material representative volume defined in terms of a periodic unit cell (PUC). Suppose that the PUC is subjected to boundary displacements $\boldsymbol{u}_0$, resulting in a uniform strain $\boldsymbol{E}$ throughout the body, Eq. (27). In view of the boundary conditions imposed on the unit cell, the strain and displacement fields in the PUC admit the following decomposition

$$\boldsymbol{u}(\mathbf{x}) = \boldsymbol{E}\cdot\mathbf{x} + \boldsymbol{u}^{*}(\mathbf{x}), \qquad \forall \mathbf{x}\in\Omega,\ \boldsymbol{u} = \boldsymbol{u}_0 \forall \mathbf{x}\in S \tag{34}$$

$$\boldsymbol{\varepsilon}(\mathbf{x}) = \boldsymbol{E} + \boldsymbol{\varepsilon}^{*}(\mathbf{x}), \qquad \forall \mathbf{x}\in\Omega. \tag{35}$$

The first term in Eq. (34) corresponds to a displacement field in an effective homogeneous medium which has the same overall properties as the composite aggregate. The fluctuation part $\boldsymbol{u}^{*}$ enters Eq. (34) as a consequence of the presence of heterogeneities and has to disappear upon volume averaging, see [Beran (1968)] for further discussion. This condition is met for any periodic displacement field with the period equal to the size of the unit cell under consideration, [Michel, et al. (1999), and references therein]. The periodicity of $\boldsymbol{u}^{*}$ further implies that the average of $\boldsymbol{\varepsilon}^{*}$ in the unit cell vanishes as well. Hence

$$\left\langle \boldsymbol{\varepsilon}(\mathbf{x})\right\rangle = \boldsymbol{E} + \left\langle \boldsymbol{\varepsilon}^{*}(\mathbf{x})\right\rangle, \qquad \left\langle \boldsymbol{\varepsilon}^{*}(\mathbf{x})\right\rangle = \frac{1}{\Omega}\int_{\Omega}\boldsymbol{\varepsilon}^{*}(\mathbf{x})\,\mathrm{d}\mathbf{x} = \mathbf{0}. \tag{36}$$

Next, assume a virtual displacement $\delta\boldsymbol{E}\cdot\mathbf{x} + \delta\boldsymbol{u}^{*}(\mathbf{x})$, with $\delta\boldsymbol{u}^{*}(\mathbf{x})$ being periodic. Then the principle of virtual work reads

$$\left\langle \delta\boldsymbol{\varepsilon}(\mathbf{x})^{\mathrm{T}}\boldsymbol{\sigma}(\mathbf{x})\right\rangle = \left\langle \delta\boldsymbol{\varepsilon}(\mathbf{x})\right\rangle^{\mathrm{T}}\left\langle \boldsymbol{\sigma}(\mathbf{x})\right\rangle = 0, \tag{37}$$

since $\left\langle \boldsymbol{\sigma}\right\rangle = \mathbf{0}$. Eq. (37) is essentially the Hill lemma introduced by Eq. (31).

Solving the above relation calls for a suitable numerical technique such as the Finite Element Method (FEM), [Bittnar &. Šejnoha (1996)]. In this framework the displacement field in Eq. (34) assumes the form

$$\boldsymbol{u}(\mathbf{x}) = \boldsymbol{E}\cdot\mathbf{x} + \mathbf{N}(\mathbf{x})\boldsymbol{r}, \tag{38}$$

where $\mathbf{N}(\mathbf{x})$ represents the shape functions of a given element, and $\boldsymbol{r}$ is the vector of the unknown degrees of freedom. The corresponding strain field is then provided by

$$\boldsymbol{\varepsilon}(\mathbf{x}) = \boldsymbol{E} + \mathbf{B}(\mathbf{x})\boldsymbol{r} \,. \tag{39}$$

Introducing Eq. (39) into Eq. (37) gives for any kinematically admissible strains $\delta\boldsymbol{\varepsilon}^* = \mathbf{B}\delta\boldsymbol{u}^*$ the associated system of linear equations in the form

$$\mathbf{K}\boldsymbol{r} = \boldsymbol{f} \,, \tag{40}$$

where

$$\begin{aligned} \mathbf{K} &= \sum_e \mathbf{K}^e \qquad \text{where} \quad \mathbf{K}^e = \frac{1}{\Omega}\int_{A^e} \mathbf{B}^{\mathrm{T}}\mathbf{L}^e\mathbf{B}\,\mathrm{d}A^e \\ \boldsymbol{f} &= \sum_e \boldsymbol{f}^e \qquad \text{where} \quad \boldsymbol{f}^e = -\frac{1}{\Omega}\int_{A^e} \mathbf{B}^{\mathrm{T}}\mathbf{L}^e\boldsymbol{E}\,\mathrm{d}A^e \,. \end{aligned} \tag{41}$$

$\mathbf{K}$ is the stiffness matrix of the system, and $\boldsymbol{f}$ is the vector of the global nodal forces resulting from the loading by $\boldsymbol{E}$; e stands for the number of elements, A^e is the area of element e and Ω is the area of the PUC.

System (40) can be used to provide the coefficients of the effective stiffness matrix $\mathbf{L}$ as volume averages of the local fields derived from the solution of the four successive elasticity problems. To that end, the periodic unit cell is loaded, in turn, by each o the four components of $\boldsymbol{E}$, while the other three components vanish. The volume stress averages normalized with respect to $\boldsymbol{E}$ then furnish the individual columns of $\mathbf{L}$. The required periodicity conditions (same displacements $\boldsymbol{u}^*$ on opposite sides of the unit cell) is accounted for through multi-point constraints.

Formulation based on stress approach

Sometimes it is desirable to apply the overall stress $\boldsymbol{\Sigma}$, Eq. (28), instead of the overall strain $\boldsymbol{E}$. Eq. (37) then modifies to

$$\left\langle \delta\boldsymbol{\varepsilon}(\mathbf{x})^{\mathrm{T}}\boldsymbol{\sigma}(\mathbf{x})\right\rangle = \delta\boldsymbol{E}^{\mathrm{T}}\boldsymbol{\Sigma}, \qquad \boldsymbol{\Sigma} = \left\langle \boldsymbol{\sigma}(\mathbf{x})\right\rangle . \tag{42}$$

Clearly, such a loading condition leaves us with an unknown overall strain $\boldsymbol{E}$ and a periodic displacement field $\boldsymbol{u}^*$ to be determined. Substituting Eq. (35) into Eq. (42) yields

$$\delta\boldsymbol{E}^{\mathrm{T}}\left\langle \mathbf{L}(\mathbf{x})\left(\boldsymbol{E} + \boldsymbol{\varepsilon}^*(\mathbf{x})\right)\right\rangle + \left\langle \delta\boldsymbol{\varepsilon}^*(\mathbf{x})^{\mathrm{T}}\mathbf{L}(\mathbf{x})\boldsymbol{E}\right\rangle + \left\langle \delta\boldsymbol{\varepsilon}^*(\mathbf{x})^{\mathrm{T}}\mathbf{L}(\mathbf{x})\boldsymbol{\varepsilon}^*(\mathbf{x})\right\rangle = \delta\boldsymbol{E}^{\mathrm{T}}\boldsymbol{\Sigma} \,. \tag{43}$$

Since $\delta\boldsymbol{E}$ and $\delta\boldsymbol{\varepsilon}^*(\mathbf{x})$ are independent, the preceding equation can be split into two equalities

$$\begin{aligned} \delta\boldsymbol{E}^{\mathrm{T}}\boldsymbol{\Sigma} &= \delta\boldsymbol{E}^{\mathrm{T}}\left[\left\langle \mathbf{L}(\mathbf{x})\right\rangle\boldsymbol{E} + \left\langle \mathbf{L}(\mathbf{x})\boldsymbol{\varepsilon}^*(\mathbf{x})\right\rangle\right] \\ 0 &= \left\langle \delta\boldsymbol{\varepsilon}^*(\mathbf{x})^{\mathrm{T}}\mathbf{L}(\mathbf{x})\right\rangle\boldsymbol{E} + \left\langle \delta\boldsymbol{\varepsilon}^*(\mathbf{x})^{\mathrm{T}}\mathbf{L}(\mathbf{x})\boldsymbol{\varepsilon}^*(\mathbf{x})\right\rangle . \end{aligned} \tag{44}$$

Finally, following the same lines as in the previous paragraph, the FE discretization (Eqs. (38) and (39)) provides the linear coupled system in the form [Michel, et al.(1999)],

$$\begin{bmatrix} \frac{1}{\Omega}\int_\Omega \mathbf{L}\mathrm{d}\Omega & \frac{1}{\Omega}\int_\Omega \mathbf{L}\mathbf{B}\mathrm{d}\Omega \\ \frac{1}{\Omega}\int_\Omega \mathbf{B}^{\mathrm{T}}\mathbf{L}\mathrm{d}\Omega & \frac{1}{\Omega}\int_\Omega \mathbf{B}^{\mathrm{T}}\mathbf{L}\mathbf{B}\mathrm{d}\Omega \end{bmatrix} \begin{Bmatrix} \boldsymbol{E} \\ \boldsymbol{r} \end{Bmatrix} = \begin{Bmatrix} \boldsymbol{\Sigma} \\ \mathbf{0} \end{Bmatrix}. \tag{45}$$

The above system of equations serves to derive the coefficients of the effective compliance matrix **M**. In analogy with the strain approach, the periodic unit cell is loaded, in turn, by each of the four components of $\boldsymbol{\Sigma}$, while the other three components vanish. The volume strain averages normalized with respect to $\boldsymbol{\Sigma}$ then supply the individual entries of **M**.

Although in the elastic regime this approach did not prove its potential, we expect the proposed approach to become irreplaceable by simple unit cells such as the periodic hexagonal array model [Teply and Dvorak (1998)] when describing the inelastic response (plasticity, damage) of material systems similar to the one under current investigation. But this has yet to be confirmed.

2.2 Unit cell on a meso-scale

Detailed numerical simulations on a micro-scale, Fig. 1(c), combined with carefully selected laboratory measurements, should offer a homogenized constitutive law for a fiber tow/epoxy matrix mixture. Such a result then allows to an accurate analysis on the meso-scale. On this level of sophistication, the computational challenge becomes obvious when examining the sample of the woven composite plate in Fig. 1(b). The periodic character of the geometry shown in Fig. 1(b) suggests the formulation of a mesoscopic representative volume element in terms of a unit cell. The main task at this level is to find the macroscopic response of the unit cell to the prescribed macroscopic strains or stresses resulting from the analysis on the macro-scale, Fig. 1(a). A macroscopic sample of a composite tube and the corresponding meso-scale unit cell are shown in Fig. 7. Essentially the same procedure as described in the previous section can be employed to carry out the numerical work.

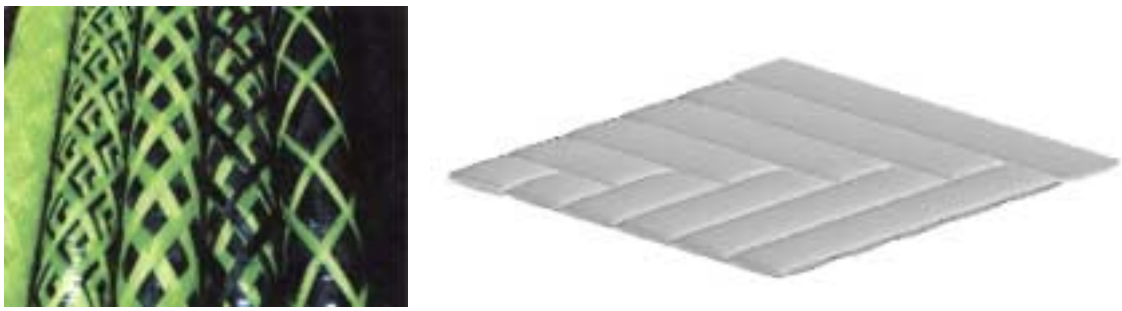

Figure 7: Modeling on meso-scale: tube sample and periodic unit cell model

The above sections suggest possible routes one may wish to consider when dealing with complex composite structures such as the one in Fig. 1. The proposed approach inevitably creates demands for efficient computational strategies and algorithms linked to a parallel environment.

3 Laboratory measurements of reinforced soils

The previous section more or less addressed the computational aspects of the multi-scale modeling of heterogeneous materials and composites in particular. A similar micromechanical view can be applied to granular materials. Novel micromechanically-based constitutive models drawing upon the deformation mechanisms taking place at grain boundaries have been introduced, among others, by [Nemat-Nasser (2000)]. Not much work if any, however, has been done in the field of soils mixed with randomly distributed reinforcements, Fig. 2(b).

To identify the basic micromechanisms driving the inelastic deformation of such materials cannot be usually done without knowledge of the macroscopic response of a soil-reinforcement composite mixture, since the macroscopic observations may pose a variety of questions which would not arise from purely micromechanical or multi-scale modeling.

This section reviews several experimental results derived for polyethylene strip reinforced soils from standard direct shear tests. The effect of the amount, shape and size of the reinforcement was considered.

A sample of clean quartz sand from Provodin with grain sizes ranging from 0.1 to 2 mm was selected for the reinforcement test. A standard laboratory direct shear test device was used to carry out the experimental measurements. Both reinforced and virgin sands were tested. The reinforced sand was prepared by mixing the sand with polyethylene strips having a width equal to 2 mm and a length of 15 and 40 mm. The squared shape of the reinforcement (2x2 mm) was also considered. The degree of reinforcement did not exceed 4 percent of the weight of the sand sample in any of the tests.

The results appear in Fig. 8. Fig. 8(a) shows variation of the shear stress as a function of the sliding displacement derived for virgin soil. The typical decay of the shear stress after its peak is evident. Fig. 8(b) displays similar results. Here, the individual lines are normalized with respect to the applied normal pressure. The figure suggests that by increasing the normal pressure, the material becomes more stable as manifested by the smaller difference between the attained shear strength and its residual value.

Figs. 8(c)-(f) show the results found for various degrees and selected shapes of reinforcement. When inspecting Fig. 8(c), it becomes clear that the small-size squared reinforcement does not improve the mechanical behavior of the mixture. On the other hand, mixing the virgin soil with strips of various sizes results in an noticeable improvement. The positive effect of an increased amount of reinforcement in the mixture evident from Figs. 8(e)-(f) is also unquestionable.

The enhancement of the material properties of the polyethylene strip-sand mixtures resulting in stable force-displacement curves is further highlighted in Figs. 9(a)-(b), which summarize the results for normal pressure equal to 100 kPa and 150 kPa, respectively. It is worthwhile to mention that the soil mixture containing longer strips with a higher degree of reinforcement did not experience undesirable material softening in any tests but rather stable behavior throughout the experiment. A slower increase in the shear stress in the initial stage can be attributed to the insufficient compaction resulting in the higher porosity of the sample. Strips of a smaller size or a lower degree of reinforcements, however, did not prevent grains from wedging. This conclusion is supported by the results displayed in Fig. 9(b), which

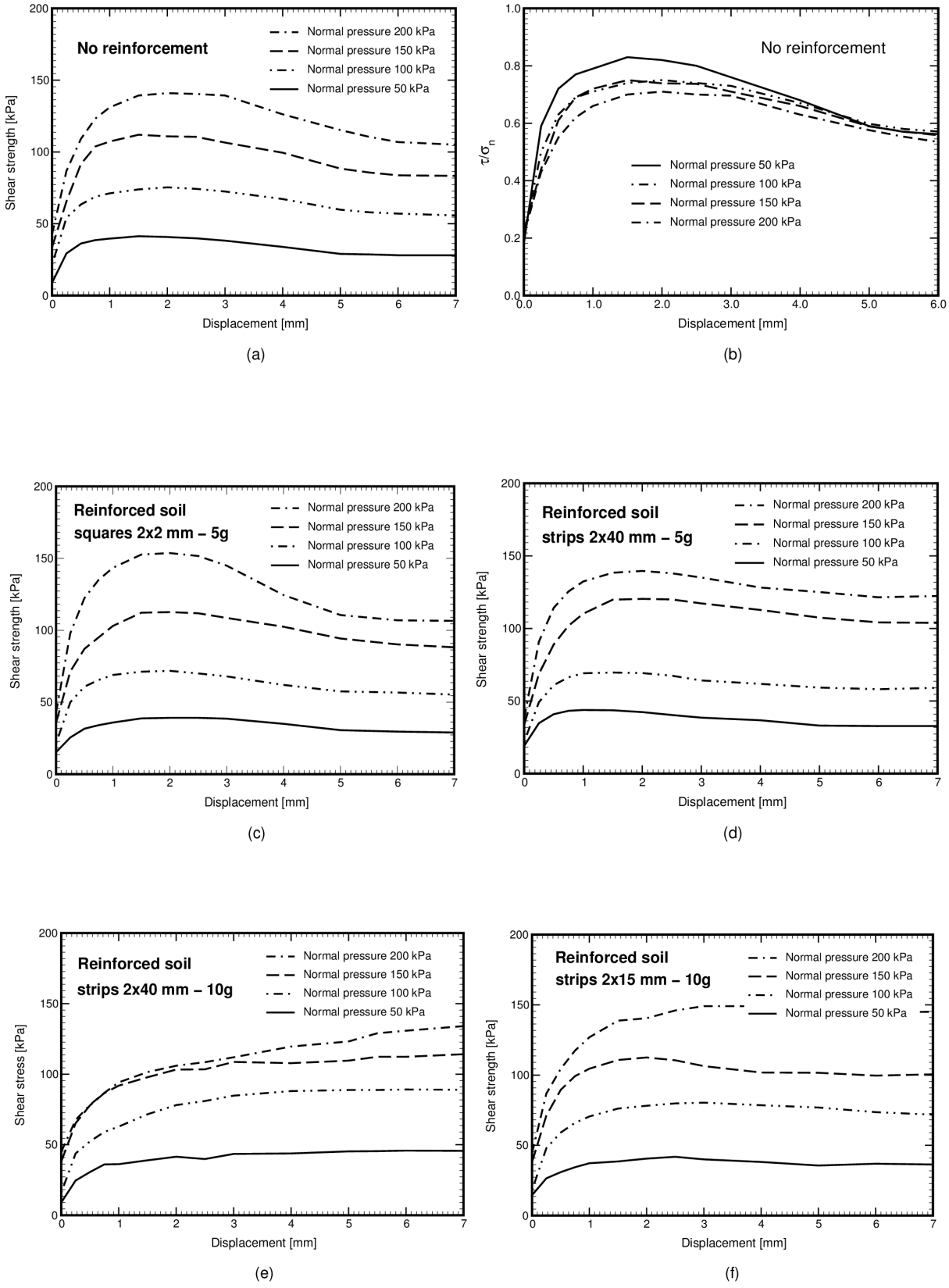

Figure 8: Direct shear stress test

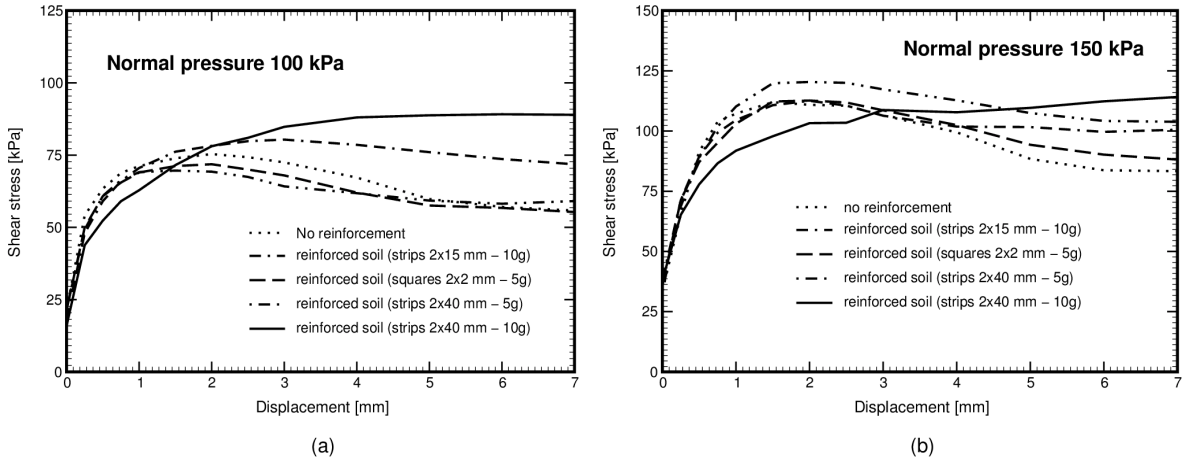

Figure 9:Direct shear stress test

correspond to the distributions already seen in Fig. 8(b). Recall the positive influence of normal pressure on soil behavior.

Although such intuitive explanations are of a certain value, more rigorous proof supported by identified deformation mechanisms is of particular interest. Moreover, the experimental measurements alone do not suffice and the back analysis is usually called to substantiate the assumptions used in the design. In this view, successful modeling of he role of the grain size, the distribution and orientation of the grains and voids, and the size and distribution of reinforcement on the macroscopic response could suggest interventions on the micro-level. Such efforts again involve modeling on different scales, starting from an evaluation of the shear resistance on the grain boundaries to assess the shear stress resistance on the meso-scale along a certain mesoscopic slip surface. Averaging over a representative volume then results in the shear resistance at a certain macroscopic point. Some data needed in such a multi-level modeling could be provided through image analyses, recall Fig. 2. In any case, identification of the micromechanisms driving the macroscopic deformation plays a vital role in the successful design of reinforced soils based on the limit equilibrium so popular among civil engineers.

4 Conclusion

Multi-scale modeling in civil engineering plays an ever-growing role as is demonstrated by two important areas of solid mechanics, composite materials and geotechnical engineering. In this paper the available theories and procedures were reviewed, and fruitful trends, particularly micromechanical analysis, were introduced.

Acknowledgment

Financial support for this work was provided by research projects CEZ: MSM 210000001,3.

References

[Beran (1968)] Beran, M.J. (1968) Statistical continuum theories, Interscience Publishers, a division of John Wiley and Sons, New York.

[Bittnar & Šejnoha (1996)] Bittnar, Z. and Šejnoha, J. (1996) Numerical methods in structural mechanics, ASCE Press and Thomas Telford Publ.

[Drugan and Willis (1996)] Drugan, W.J. and Willis, J.R. (1996) A micromechanics-based nonlocal constitutive equation and estimates of representative volume element size for elastic composites, *J. Mech. Phys. Solids*, **44 (4)**, pp. 497-524

[Gray & Ohashi (1983)] Gray, D.H., Ohashi H., (1983) Mechanics of fiber reinforcement in sand, *J. Geotech. Engr.*, ASCE, **109(3)**, pp. 335-353.

[Hashin & Shtrikman (1963)] Hashin, Z. and Shtrikman, S. (1963) A variational approach to the theory of elastic behavior of multiphase materials, *J.Mech. Phys. Solids*, **11**, pp. 127-140.

[Hill (1963)] Hill, R. (1963) Elastic properties of reinforced solids: {Some theoretical principles, *JMPS*, **11**, pp. 357-372.

[Michel, et al. (1999)] Michel, J.C. and Moulinec, H. and Suquet, P. (1999) Effective properties of composite materials with periodic microstructure: {A computational approach, *Computer Methods in Applied Mechanics and Engineering*, **172**, pp. 109-143.

[Nemat-Nasser (2000)) Nemat-Nasser, S. (2000) A micromechanically-based constitutive model for frictional deformation of granular materials, *J. Mech. Phys*. Solids, **48**, pp. 1541-1563.

[Sejnoha, et al. (1999)] Šejnoha, M., Horečka, L. and Matouš, K. (1999) Modeling of masonry structures strengthened by pre-tensioned glass-fiber-reinforced polymer laminates, *Computational methods and experimental measurements IX*, editors: G.M. Carlomagno, C.A. Brebia, WITpress, Sorrento 1999, pp. 381-390.

[Šejnoha (2000)] Šejnoha, M. (2000) Micromechanical analysis of random composites. Habilitation thesis, CTU Prague.

[Sejnoha, et al. (2000)] Šejnoha, M., Zeman, J. and Šejnoha, J. (2000) Evaluation of effective thermal properties of random composites via periodic fields, presented at *3rd International Congress of Croatian Society of Mechanics*, 28-30 September, 2000, pp. 427-334, Dubrovnik, Croatia.

[Tarliozs, et al. (1998)] Tatlisozs, N., Edil, T.B., Benson, C.H., (1998) Interaction between reinforcing geosynthetics and soil-tire chip mixtures, *J. Geotech. and Env. Engr.*, **124(11)**, pp. 1109-1119.

[Teply and Dvorak (1988)] Teply J.L. and Dvorak G.J. (1988) Bounds on overall instantaneous properties of elastic-plastic composites, *J. Mech. Phys. Solids*, **36**, pp. 29-58.

[Torquato and Stell (1985)] Torquato, S. and Stell, G. (1985) Microstructure of two-phase random media. V. The *n*-point matrix probability functions for impenetrable spheres, *Journal of Chemical Physics*, **82(2)**, pp. 980-987.

[Torquato (1991)] Torquato, S. (1991) Random heterogeneous media: Microstructure and improved bounds on effective properties, *Appl. Mech. Rev*., **44(2)**, pp. 37-76.

[Zeman et al. (2000)] Zeman, J., Šejnoha, J. and Šejnoha, M. (2000) Effective properties of statistically homogeneous random composites, presented at *CADCOMP 2000*, pp. 143-152, Bologna, Italy.

[Zeman & Sejnoha (2001)] Zeman, J. and Šejnoha, M. Numerical evaluation of effective elastic properties of graphite fiber tow impregnated by polymer matrix, in *J. Mech. Phys. of Solids*., **49**, pp. 69-90.